Open access • Journal Article • DOI:10.1080/08927020802353491

Carbon nanotube assisted water self-diffusion across lipid membranes in the absence and presence of electric fields — Source link

Don James MacElroy, Jose Antonio Garate, Niall J. English

Published on: 23 Jan 2009 - Molecular Simulation (Taylor & Francis Group)

Topics: Membrane, Carbon nanotube, Permeation and Electrostatics

Carbon nanotube assisted water self-diffusion across lipid membranes in the absence and presence of electric fields

Don James Macelroy, Jose-Antonio Garate, Niall J. English

Molecular Simulation
Journal of
Experimental Nanoscience

Taylor & Francis
Taylor & Francis Group

Carbon nanotube assisted water self-diffusion across lipid membranes in the absence and presence of electric fields

Journal:	*Molecular Simulation/Journal of Experimental Nanoscience*
Manuscript ID:	GMOS-2008-0112.R1
Journal:	Molecular Simulation
Date Submitted by the Author:	10-Jul-2008
Complete List of Authors:	MacElroy, Don; University College Dublin, Chemical and Bioprocess Engineering Garate, Jose-Antonio; University College Dublin, Chemical and Bioprocess Engineering English, Niall; University College Dublin, Chemical and Bioprocess Engineering
Keywords:	Water self-diffusion, Carbon nanotubes, Lipid membranes

Carbon nanotube assisted water self-diffusion across lipid membranes in the absence and presence of electric fields

J.-A. Garate, N.J. English and J.M.D. MacElroy[a]

The SEC Strategic Research Cluster and the Centre for Synthesis and Chemical Biology, UCD School of Chemical and Bioprocess Engineering, University College Dublin, Belfield, Dublin 4.

Abstract

Water self-diffusion has been investigated by molecular dynamics (MD) simulation through armchair single walled carbon nanotubes (SWCNTs) implanted in 1-palmytoil-2-oleoyl-sn-glycero-3-Phosphatidylcholine (POPC) membrane patches. Four systems were investigated, each containing one of (5,5), (6,6), (8,8) and (11,11) CNTs with diameters of 6.89, 8.20, 11.04 and 15.02 Å and a length of 36.9 Å, oriented normal to the membrane. The CHARMM 27 potential was used, in conjunction with TIP3P water, with particle-mesh Ewald electrostatics. Equilibrium and non-equilibrium MD simulations were performed in the respective absence and presence of a static electric field with an intensity of 0.0065 V/Å, applied along the axis normal to the membrane, *i.e.* approximately along the axis of the CNTs. It was found that the permeation rate of tracer water molecules was enhanced from 1.13 particles per nanosecond to 2.6 particles per nanosecond in the presence of the field in the case of the (5,5) CNT, whilst the permeation rate per unit area declined in the larger nanotubes vis-à-vis equilibrium zero-field conditions. Single-file diffusion was observed in the (5,5) and (6,6) cases, compared to classical diffusion in the larger pores. From an analysis of the molecular dipole moment distributions, the number of water molecules present in the CNTs, and the hydrogen bonding characteristics of water inside the CNTs and at their mouth, these trends have been rationalised. A significant decrease in the fluctuations in the number of water molecules in the (5,5) CNT due to enhanced dipole alignment in the electric field resulted in an increased rate of incorporation of the water molecules into this CNT, whereas sharper alignment of the water dipoles with the field coupled with the greater rotational freedom of the water molecules in the (6,6) nanotube tended to reduced water self-diffusion.

[a] Corresponding author: e-mail: Don.MacElroy@ucd.ie; Fax: 353-1-716 1177

Keywords: Water self-diffusion; Carbon nanotubes, Lipid membranes

1. Introduction

In the last twenty five years the molecular simulation of transport process in inhomogeneous media and nanoporous structures, ubiquitous to many physical, chemical and biological systems, has grown rapidly. In particular, recent work has focussed on water transport within biological membranes (for example aquaporins [1,2], gramicidin-like channels [3]) and simplified models of these systems (single carbon nanotubes (CNTs) or arrays of CNTs [1, 4-10]). The work on CNTs is of significant interest in that these materials display a simplicity of behaviour which permits a clearer understanding of the mechanics of the transport processes taking place in more complex biological media. For example, in [5] Zhu and Schulten simulate an hexagonal array of (6,6) armchair CNTs with four basic charge conformations including two interesting bipolar charge configurations which are considered to be representative of the electrostatic fields in biological channels (most notably as simple models of aquaporins). The authors observe that the charge electrostatic fields within the channels give rise to particular water dipole orientations that ultimately have a significant effect on the permeation rates. The observed rates are discussed in light of the continuous-time random walk (CTRW) model of Berezhkovskii and Hummer [4] which predicts that the permeation rate, j, for water tracer molecules undergoing unidirectional single-file diffusion is (see also [1])

$$j = \frac{pv_w}{2}\Delta c_{tr} = \frac{v_w k}{2(N+1)}\Delta c_{tr} = \frac{v_w k_0}{N+1}\Delta c_{tr} \qquad (1)$$

where v_w is the average volume of a single water molecule, p and k are the number of bi-directional permeation events per unit time and the bi-directional hopping rate respectively, k_o is the unidirectional hopping rate and N is the number of water molecules in the channel. In [1, 4, 5] the average hopping rate is generally related to the intrapore self-diffusion coefficient, D_p, by

$$k = 2D_p / a^2 \qquad (2)$$

where D_p is computed from the mean square displacement of the water molecules inside the nanotubes and a is the average spacing between the water molecules. The results reported by Zhu and Schulten for (6,6) channels 1.34nm in length (with loadings corresponding to 5 water molecules) were in good agreement with the above expressions.

Additional studies [1, 6, 7] have examined pressure driven water flows across membranes composed of arrays of (6,6) single-file CNTs and larger CNTs (see [8] and others cited therein). The results in all cases demonstrate that the convective flows are very high and that the transport process is close to frictionless within the nanotubes in view of their relatively smooth walls at an atomic scale. While convective flow is not investigated in the work to be reported below the observation of the absence of any significant barriers to transport within the CNTs will be relevant to the discussion of the results to be presented later.

In this paper we report further studies of unidirectional single-file diffusion of water within (5,5) and (6,6) CNTs and classical diffusion of water in (8,8) and (11,11) CNTs. The latter provide insight into the transitional behaviour of the diffusional flux as the transport mechanism changes from single-file to classical. The (5,5) and (6,6) CNT studies on the other hand will serve to assess the validity of Equation (1) in light of recent results reported by Li et al [9]. Computations are also reported for diffusion in the presence of a static electric field highlighting shortcomings in the simplified approach described by Equations (1) and (2). The CNTs were embedded in a bilayer membrane to imitate the influence of a relevant biological 'background' on the diffusional properties of water. Although the explicit influence of the head groups upon water diffusion is beyond the scope of this paper, we intend to examine this in some detail in future work.

2. Simulation Methods and Modelling

Simulation Methods

All simulations were performed using the MD program NAMDv2.6b [11] and the CHARMM27 parameter set [12]. The rigid TIP3P water model [13] was used, as the CHARMM27 set was parameterized in conjunction with this potential. Four periodically replicated simulation cells were investigated, with each one consisting individually, respectively, of (5,5), (6,6), (8,8) and (11,11) armchair single walled carbon nanotubes (SWCNT's) with diameters of 6.89, 8.20, 11.04 and 15.02 Å and an approximate length of 36.9 Å; each was embedded in a 1-palmytoil-2-oleoyl-sn-glycero-3-Phosphatidylcholine (POPC) membrane patch, with layers of solvation water molecules of about 10 Å in length in the $+z$ and $-z$ directions (*i.e.* 'above' and

'below' the membrane patch, cf. Fig. 1). The finite-size SWCNT´s were constructed using the program CoNTubv1.0 [14], with each atom of the CNT modeled as a neutral sp^2 aromatic carbon, with uncapped ends. For all of the systems, the POPC membrane plane was placed in the *x*-*y* plane and the axis normal to the membrane was along the *z*-direction with the CNT oriented along the normal to the membrane. The periodic cell size for the (5,5) and (6,6) CNT cases was 35x35x70 $Å^3$ with total atom numbers of 8,780 and 8,415, respectively, whilst the (8,8) and (11,11) CNT systems consisted of a periodic cell of 45x45x70 $Å^3$ with 13,882 and 13,659 atoms, respectively. Each of these systems were built using the program VMDv1.86 [15].

The Particle Mesh-Ewald method [16] was used to compute long-range electrostatics to within a relative tolerance of $1x10^{-6}$; it was found that a real-space screening coefficient of 0.258 $Å^{-1}$ and grid spacings in the 0.9 to 1 Å range in each Cartesian direction offered this desired level of accuracy together with close-to-optimal execution speed. A cut-off distance of 12 Å was applied to real-space Ewald interactions. The same value was used for van der Waals interactions, with a smooth switching function applied thereto between 10 and 12 Å. The SHAKE algorithm [17] was applied to constrain bond lengths to hydrogen atoms and to maintain the rigid TIP3P geometry. A time step of 1 fs was used with the velocity Verlet scheme [18]. For MD in the NVT ensemble, Langevin dynamics [19] was applied with a set point of 300 K and a damping coefficient of 1 ps^{-1}. For MD in the NPT ensemble, the Nose-Hoover method was applied [20] with anisotropic cell variation, using Langevin dynamics for piston fluctuation control [21], with set points of 1 atm and 300 K. Hydrogen bonds were identified by geometric criteria: a water pair is considered to be hydrogen bonded if the oxygen-oxygen distance is less than 3.5 Å and the O-H···O angle is greater than 150°, with all O-H···O angles classified as being between 0 and 180° [22].

Prior to production simulations, a 1 ns NPT relaxation run was performed with CNT atoms fixed and the lipid bilayer and water molecules moving freely. Following this, the CNT atoms were released slowly, maintaining a harmonic constraint thereon with a coefficient of 1 kcal/mol·$Å^2$. This coefficient was reduced every 100 ps for 0.4 ns down to 1.5, 1.0 and 0.5 kcal/mol·$Å^2$. After initial relaxation, equilibrium MD simulations were performed in the NPT ensemble on the systems containing the (5,5)

and (6,6) CNT's for 30 ns, and for 20 ns in the case of the (8,8) and (11,11) CNT's, whilst maintaining a light harmonic constraint on the CNT atoms (with a coefficient of 0.5 kcal/mol·Å²). The first 5 ns were considered as further relaxation, keeping the rest of the simulation time as production run.

To investigate the influence of external static electric fields on water self-diffusion, non-equilibrium MD simulations were carried out in an electrical field with an intensity of 0.0065 V/Å applied in the -*z* direction. In this case, the force exerted by the field on partial atomic charges *ia* is given by

$$\boldsymbol{f}_{ia} = q_{ia}\boldsymbol{E}$$

After observing instability of the lipid bilayer at substantially larger field intensities (of the order of 0.1 V/Å), the value of 0.0065 V/Å was selected. It was desired to assess a lower field intensity for longer periods of tens of nanoseconds, as this is in closer accord to experimental conditions, and the fully flexible bilayer was found to be stable under these field conditions. This field corresponds to a voltage difference of approximately 240 mV across the 3.7 nm membrane, which, although larger than typical membrane potentials of 60 to 100 mV, is still in the physiological range. The same configurations from the initial relaxation protocol were used as input to the non-equilibrium simulations, except that these were carried out in the NVT ensemble to avoid any problems with too rapid dilation of the system volume in the relatively weak electric field.

No restraints were applied to the bilayer, while a light 0.5 kcal/mol.Å^2 harmonic constraint was applied to the CNT atoms, in both the absence and presence of the electric fields. In particular, the neutral state of the CNT atoms led to no direct movement imparted thereon by the field (cf. equation above). Although Newsome and Sholl [23] have recommended with good justification the use of local thermostats to maintain appropriate isothermal conditions in the case of diffusion through fixed geometries, the mild harmonic restraints applied to the CNT in this study, coupled with the fully flexible bilayer, suggest that the thermostat used is reasonable. It is considered beyond the scope of this paper to conduct a detailed study on the effects of thermostatting procedures on diffusion, but we intend to examine the influence of

damping coefficients and of local and global application of thermostats on diffusion in future work.

Figure 2 illustrates the structure of the periodic cell for the analysis of the self-diffusion permeation rates for water within the CNTs described above. The periodic cell is imaged in all directions with a 'black' particle reservoir to the left and a 'white' particle reservoir to the right, both a distance L from the respective CNT pore mouths. The steady-state counter-diffusion of both species is monitored through the x-y plane located at $z = 0$ within the CNT. 'Black' particles diffusing to the right are converted to 'white' once they enter the white reservoir and vice versa for the white particles. If a black particle diffuses from the left hand reservoir across the periodic boundary at $z = -L_c$ it enters as a white particle on the right hand side. In all of the simulations conducted here L was taken 0.6 nm.

Simplified diffusion/kinetic rate model

To model the diffusion process, consider the flux of the 'black' water molecules from left to right in Figure 2 (a similar analysis applies to 'white' diffusion). If the cross-sectional area in the bulk is A and the cross-section in the pore is A_p and L is the length of the mixing zone between the black reservoir and the pore mouth, then at steady state the net flow (particles per unit time) between the black reservoir and the outer perimeter of the CNT is simply

$$j_B = \frac{DA}{L}(c_1 - c_2) \qquad (3)$$

where c_1 is the concentration of black water molecules in the black reservoir and c_2 is the concentration of black water molecules just outside the CNT pore mouth.

At the pore mouth we consider a simple reversible rate process for the molecules to either enter the pore or return into the bath on the left i.e. the net rate is

$$r_{2-2p} = k_f c_2 - k_r c_{2p} \qquad (4)$$

With k_i (forward and reverse hopping rates) in units of sec^{-1} and c_{2p} is the concentration of black water molecules just inside the CNT pore adjacent to the pore mouth. The above net rate is a volumetric measure (these rate constants will be determined to a great extent by the hydrogen bond structure and dynamics). Multiplying by a volume V_i (an interfacial volume corresponding to $A_p\delta$ with δ =

length scale of the order of the molecular dimensions representing the scale of the concentration inhomogenities) then for steady state conditions we have

$$V_i r_{2-2p} = V_i(k_f c_2 - k_r c_{2p}) = V_i k_f (c_2 - \frac{1}{K_p} c_{2p}) = j_B = \frac{DA}{L}(c_1 - c_2)$$

Eliminating c_2 from this set of equations we have simply

$$j_B = \frac{p_1}{K_p}(K_p c_1 - c_{2p}) \qquad (5)$$

where K_p is defined as k_f/k_r and p_1 is the partial permeability for diffusive transport from the black reservoir to just inside the CNT:

$$\frac{1}{p_1} = \frac{L}{DA} + \frac{1}{k_f V_i}$$

Defining a diffusion coefficient, D_p, within the pore (which is considered to exist in the same sense as proposed in [1, 4, 5] but which has a deeper meaning than indicated by the simple CTRW, as discussed towards the end of Section 3) then

$$j_B = \frac{D_p A_p}{L_p}(c_{2p} - c_{3p}) \qquad (6)$$

where L_p is the length of the pore and c_{3p} is the concentration of black water molecules just inside the CNT pore adjacent to the pore mouth near the white particle reservoir.

Also, for the right hand side of the system it follows from Equation (5) that

$$j_B = \frac{p_1}{K_p}(c_{3p} - K_p c_4) \qquad (7)$$

where c_4 is the concentration of black water molecules in the white particle reservoir.

Now combining (5), (6) and (7) appropriately to eliminate the intermediate concentration terms between the reservoirs gives

$$j_B = p(c_1 - c_4)$$

where

$$\frac{1}{p} = \frac{2}{p_1} + \frac{L_p}{D_p K_p A_p} = \frac{2L}{DA} + \frac{2}{k_f V_i} + \frac{L_p}{D_p K_p A_p} \qquad (8)$$

A physical interpretation of Equation (8) is that the permeability is governed by a sum of mass transfer resistance terms due to bulk diffusion, incorporation into the pore

mouth and intrapore diffusion. Normally one sets $\boldsymbol{c}_4 = 0$ and $\boldsymbol{c}_1 = \boldsymbol{c}_{H2O}$ = molar density of water in the bulk. The overall permeability can be simply determined from the MD simulations and by selecting different positions for the 'black' and 'white' reservoirs one can eliminate the bulk diffusion (*D/L)* terms.

To compare with the simplified CTRW, note that implicit in the CTRW model is the assumption that L is sufficiently small to minimise bulk phase diffusional resistance while retaining a subnanometer range close to the pore mouth ($\delta \sim a$) to ensure that entry/exit kinetics are fully taken into consideration. This condition with the additional assumption that the single file is considered to be densely packed leads to

$$L_p = Na;\ \delta = a$$

where a is a length scale characteristic of the size of the water molecules. Furthermore, the diffusion coefficient within the pore is also assumed in the CTRW model to be given by

$$D_p = \frac{a^2}{2\tau} = \frac{a^2}{2} k_r \qquad (9)$$

We note further here that we make the distinction that the intrapore hopping rate k is equal to k_r i.e. the reverse rate constant in Equation (4). Within the pore, the forward and reverse hopping rate constants are equal; however it is important to recognise that the forward rate constant in Equation (4) which represents the rate at which water molecules enter the pore is not equal to k_r and that for the CNTs under consideration here one may anticipate $k_r > k_f$ or $K_p < 1$. Subject to these conditions and assuming the molecular volume $v_w = aA_p$ we find

$$\text{Permeation rate} = \frac{k_f a A_p}{2} \frac{1}{N+1} c_{H2O} = \frac{v_w k_o}{N+1} \Delta c_{H2O} \qquad (10)$$

which is the simple CTRW result given in Equation (1). This analysis demonstrates the level of the assumptions involved in the CTRW approach. As noted above, in a more general setting, the in-pore forward hopping frequency is not the same as at the pore mouth. Furthermore, the more general model of Equation (8) applies to wide (i.e. multi-pass) pore conditions of arbitrary cross-sectional area and it is also simple to

extend Equation (8) to include rate processes at other junctions (e.g. local charged sites) within the pore and to relate the rate constants to the energy barriers associated with the particle movement along the channel.

3. Results

The results for the steady state unidirectional permeation rates (in number of water molecules per nanosecond) in the absence and in the presence of the static electric field are provided in Table 1 (note that the bulk resistance term $2L/DA$ in Equation (8) is negligible in these studies amounting to approximately 1.3% of the overall resistance in the worst case for the largest pore). The zero field results exhibit a monotonic increase with pore radius as might be expected and the data have been scaled in the fourth column of this table to illustrate this. The influence of the electric field however is quite clearly evident in third and last columns of this table. To gain insight into the phenomena which lead to these results let us first consider the zero field data. In Table 2 we report the intrapore self-diffusion coefficients computed using

$$D_p = \lim_{t\to\infty} \frac{1}{2} \frac{d\left\langle (\Delta z)^2 \right\rangle}{dt}$$

with the mean square displacement (MSD) averaged over many time origins and determined from the particle trajectories for the period in which those particles originating at the centre of the pore remained within the pore (5 sample bins were employed in computing the standard errors in each case reported in Table 2). In all cases it was observed that after an initial sub-diffusion regime, the trajectories were linear (Fickian) for times $t \geq 20$ ps (the MSDs for the two extreme cases of the (5,5) and (11,11) channels are provided in Figure 3 to illustrate the transition from sub-diffusion to the Fickian regime at approximately 20 ps). Rescaling the particle fluxes using the self-diffusion coefficients suggests that the intrapore diffusion or hopping rate, k_r (see Equation (9)) controls the magnitude of the diffusion flux for all pore sizes including single-file and classical diffusion conditions.

As an aside we would like to note that for colour diffusion the distinction of transport diffusivity and self-diffusivity is not required since both are strictly equal under these special conditions. Only if a physical difference exists between the two

counterdiffusing species (e.g. mass, particle diameter/shape, or potential interaction) will this distinction arise. The colour particle diffusivity D_p in Equation (8) is precisely the same as the self-diffusivity computed from the derivative of the single-particle mean-square displacement and is independent of concentration. Also in view of the ideality of this special mixture the Darken factor is simply equal to 1.0.

Furthermore if we assume, in keeping with the simplified lattice theory for diffusion in liquids, that generally $V_i = aA_p$ then Equation (8) may be expressed as follows after neglecting the bulk diffusion term

$$p = D_p K_p \frac{A_p}{a + L_p} \tag{11}$$

From the second last column of Table 2 it is clear that since the ratio of the rate constants $K_p = k_f / k_r$ is essentially independent of the pore size for the three smallest pores, the pore-entry hopping rate is strongly coupled with the internal hopping rate within the pore in agreement with earlier work on water transport within single-file (6,6) CNTs [1, 4-7]. The larger value for the (11,11) CNT reflects approach to the the limiting condition $K_p \to 1$ as the fluid within the pore and at the pore mouth assume properties characteristic of the bulk state.

In the presence of the electric field the results shown in Tables 1 and 2 demonstrate that the pore-entry and intrapore hopping rates are to some extent decoupled particularly for the two single-file pores (5,5) and (6,6). The drop in the permeation rate for the (6,6) pore is consistent with similar observations by Zhu and Schulten [5] for a model (6,6) CNT with fixed charges of –0.5e and +0.5e at respective ends of their 1.34 nm long nanotube. The influence of the electric field on the probability distribution of the angle of the water dipoles with respect to the (positive) z-axis, θ, within our (5,5) and (6,6) pores is illustrated in Figure 4. In agreement with Zhu and Schulten we find that the orientational distributions of the dipoles in the absence of the field are symmetric with peaks at ±1 demonstrating that the dipoles of all the water molecules in the single file simultaneously point either in the $-z$ or $+z$ directions. In the presence of the static e-field, the distribution is shifted almost entirely to the left of the diagrams. In the case of the (5,5) CNT there is a weak maximum in the region of $\cos\theta = +1$ while no such maximum exists for the (6,6)

pore. The strongly hindered rotational motion in the (5,5) pore is the reason for this since the water molecules fit very snugly within this CNT (the effective diameter of the (5,5) pore is (d_p – 0.34) = 0.349 nm which is nearly equal to the oxygen Lennard-Jones diameter, 0.315 nm, for the TIP3P model - see, for example, Figure 1c). For the (6,6) pore the space is far less restricted with an effective pore diameter of 0.48 nm and the dipoles can readily align with the electric field.

The jump in the value for K_p shown for the (5,5) pore in the last column of Table 2 is closely related to the hindered rotational motion of the water molecules within this pore and to an additional feature of the water loading of the pore as shown in Figure 5. In this figure we plot the distribution of the intrapore loadings and the number of hydrogen bonds for the entire MD simulations. With the exception of the (5,5) pore, the field has little effect on these properties. In the (5,5) pore, however, we note that the average number of water molecules within the pore in the absence of the field is generally lower than when the field is turned on. In this pore, while H-bonding is weakest, dipole alignment induced by the field results in a noticeable reduction in the fluctuations in particle numbers which are clearly observed in the absence of the field. A careful examination of a large number of snapshots of pore loadings in both the zero-field and full-field simulations for this pore demonstrated that clusters of misaligned dipoles occurred with high frequency in the zero-field case but were largely absent under e-field conditions. This results in a greater frequency of jumps into the pore (high k_f) with only a marginal, if any, effect on the reverse jump rate governed by k_r as implied by the diffusion coefficients D_{p0} and D_{pE}.

Before concluding we consider a brief comparison of the non-field (6,6) results with those reported in [4, 5, 9]. The results we have obtained are qualitatively similar to those reported in [4, 5]. Since the pore lengths differ by a factor of 3 we compare the hopping rates provided by D_p. In our case we find k (= k_r) = 69.5 ns^{-1} while for similar thermodynamic conditions Berezhkovskii and Hummer [4] report 76.9 ns^{-1} and Zhu and Schulten [5] give 26.9 ns^{-1}. It is of interest to note that our result is in very good agreement with Berezhkovskii and Hummer who employed the TIP3P model for water interactions and AMBER for the CNT, in contrast to the TIP3P/CHARMM potential modelling which both our results and the results reported by Zhu and Schulten are based on. We believe the much lower hopping rates observed

in [5] are due to the array of parallel nanotubes employed by the latter in their work. The single-files of water within the twelve closely packed CNTs in [5] interact with one another via long-range electrostatic interactions causing friction which retards the rate of movement of the individual files (on average half of the water files are moving counter to the remaining half).

A final point of interest is the qualitative verification of Equation (1) and (2) for our long pore results. Retaining the CTRW assumption that $K_{p0} = 1$ and using only the results provided in Table 2 for D_p to estimate k with the hopping length scale a = 0.26nm, we find for the (5,5) and (6,6) pores that Equation (1) predicts j = 1.59 ns^{-1} (5,5) and j = 3.39 ns^{-1} (6,6) in fair agreement with the full colour diffusion simulations (the primary reasons for the discrepancy rests with the assumption $K_{p0} = 1$). This is in sharp contrast to the results reported by Li et al [9] who suggest that the permeation rates are lower by a factor of 4 due to a pore-length dependence related to the decay in correlations associated with pore-entry and pore-exit hopping events. We observe no such dependence and we suggest that the lack of such a relationship (in contrast to the influence of pore-length suggested for stochastic diffusion processes in other sources [24-27]) does not exist due to the 'frictionless' nature of the water molecule interactions with the CNT pore walls. Our results do conform, however, to ideal one-dimensional diffusion in a confined tubular space with specularly reflecting (axial momentum conserving) walls as suggested by the results of Lebowitz and Percus [28].

4. Conclusions

The results reported in this work for single-file pores in the absence of fields are in fair agreement with the CTRW of Berezhkovskii and Hummer [4] although discrepancies are observed particularly in the presence of electric fields. In this regard, it has been shown that self-diffusion of water molecules through a (5,5) CNT embedded in a lipid bilayer is significantly enhanced by static electric fields, in contrast to CNTs of larger diameter. The electric field intensity of 0.0065 V/Å is weak in comparison to previous molecular simulation studies employing static and time-varying fields [29, 30] and is also weak relative to fields generated by charge distributions [5]. A significant decrease in the fluctuations in the number of water

molecules in the (5,5) CNT upon application of the field facilitates the incorporation of a larger number of water molecules in the CNT, whereas the greater rotational freedom of water molecules in the (6,6) tube, and in larger CNTs, permits enhanced alignment of their dipoles with the field resulting in a reduced water self-diffusion flux. In future work we will examine this in greater detail and extend this work to investigate the influence of time-varying far infrared and microwave fields on the properties of water confined within model CNTs of various sizes in addition to the influence of head groups on water diffusion.

References

[1] E. Tajkhorshid, F. Zhu and K. Schulten, 'Kinetic Theory and Simulation of Single-Channel Water Transport', Ch. 5.15, in *Handbook of Materials Modeling* (Ed. S. Yip), Springer, Netherlands, 2005, 1797-1822.

[2] M. Hashido, A. Kidera and M. Ikeguchi, 'Water transport in Aquaporins: Osmotic Permeability Matrix Analysis of Molecular Dynamics Simulations', Biophys. J., **93** (2007) 373-385.

[3] G. Portella, P. Pohl and B.L. de Groot, 'Invariance of Single-file Water Mobility in Gramcidin-like Peptidic Pores as Function of Pore Length', Biophys. J., **92** (2007) 3930-3937.

[4] A. Berezhkovskii and G. Hummer, 'Single-file Transport of Water through a Carbon Nanotube', Phys. Rev. Lett., **89** (2002) 064503-1-4.

[5] F. Zhu and K. Schulten, 'Water and Proton Conduction through Carbon nanotubes as Models of Biological Membranes', Biophys. J., **85** (2003) 236-244.

[6] F. Zhu, E. Tajkhorshid and K. Schulten, 'Collective Diffusion Model for Water Permeation through Microscopic Channels', Phys. Rev. Lett., **93** (2004) 224501-1-4.

[7] A. Kalra, S. Garde and G. Hummer, ' Osmotic Water transport through Carbon Nanotube Membranes', Proc. Natl. Acad. Sci. U.S.A., **100** (2004) 10175-10180.

[8] S. Joseph and N.R. Aluru, 'Why are Carbon Nanotubes Fast Transporters of Water?', Nano Lett., **8** (2008) 452-458.

[9] J.-Y. Li, Z.-X. Yang, H.-P. Fang, R.-H. Zhou and X.-W. Tang, 'Effect of the Carbon Nanotube Length on Water Permeability', Chinese Phys. Lett., **24** (2007) 2710-2713.

[10] B. Mukherjee, P.K. Maiti, C. Dasgupta and A.K. Sood, 'Structure and Dynamics of Confined Water Inside Narrow Carbon Nanotubes', J. Nanosci. Nanotechnol., **7** (2007) 1796-1799.

[11] J.C. Phillips, R. Braun, W. Wang, J. Gumbart, E. Tajkhorshid, E. Villa, C. Chipot, R.D. Skeel, L. Kale and K. Schulten, 'Scalable molecular dynamics with NAMD', J. Comp. Chem., **26** (2005)1781-1802.

[12] A.D. MacKerell Jr., D. Bashford, M. Bellott, R.L. Dunbrack Jr, J.D. Evanseck, M.J. Field, S. Fischer, J. Gao, H. Guo, S. Ha, D. Joseph–McCarthy, L. Kuchnir, K. Kuczera, F.T.K. Lau, C. Mattos, S. Michnick, T. Ngo, D.T. Nguyen, B. Prodhom, W.E. Reiher III, B. Roux, M. Schlenkrich, J.C. Smith, R. Stote, J. Straub, M. Watanabe, J. Wiorkiewicz–Kuczera, D. Yin and M. Karplus, 'All-hydrogen empirical potential for molecular modeling and dynamics studies of proteins using the CHARMM22 force field', J. Phys. Chem. B, **102** (1998) 3586–3616.

[13] W.L. Jorgensen, J. Chandrasekhar, J.D. Madura, R.W. Impey and M.L. Klein, 'Comparison of simple potential functions for simulating liquid water', J. Chem. Phys., **79** (1983) 926-935.

[14] S. Melchor and J.A. Dobado, 'CoNTub: an algorithm for connecting two arbitrary carbon nanotubes', Inf. Comput. Sci., **44** (2004) 1639-1646 (2004).

[15] W. Humphrey, A. Dalke and K. Schulten, 'VMD-Visual Molecular Dynamics', J. Molec. Graphics, **14** (1996) 33-38.

[16] T. Darden, D. York and L. Pedersen 'Particle Mesh-Ewald: An Nlog(N) method for Ewald sums in large systems', J. Chem. Phys.**98** (1993) 10089–10092.

[17] J.P. Ryckaert, G. Ciccotti and H.J.C. Berendsen, 'Numerical integration of the Cartesian equations of motion of a system with constraints: molecular dynamics of *n*-alkanes', J. Comp. Phys., **23** (1977) 327–341.

[18] M.P. Allen and D.J. Tildesley, D.J., *Computer Simulation of Liquids,* Oxford: Clarendon Press, 1987.

[19] G.S. Grest and K. Kremer, 'Molecular-dynamics simulation for polymers in the presence of a heat bath', Phys. Rev. A, **33** (1986) 3628–3631.

[20] G.J. Martyna, D.J. Tobias and M.L. Klein, 'Constant pressure molecular dynamics algorithms', J. Chem. Phys., **101** (1994) 4177–4189.

[21] S.E. Feller, Y. Zhang, R.W. Pastor and B.R. Brooks, 'Constant pressure molecular dynamics simulation: the Langevin piston method', J. Chem. Phys., **103** (1995) 4613–4621.

[22] A. Luzar and D. Chandler, 'Effect of Environment on Hydrogen Bond Dynamics in Liquid Water', Phys. Rev. Lett., **76** (1996) 928-931.

[23] D.A. Newsome and D.S. Sholl, 'Predictive Assessment of Surface Resistances in Zeolite Membranes Using Atomically Detailed Models', J. Phys. Chem. B, **109** (2005) 7237-7244.

[24] J.M.D. MacElroy and S.-H. Suh, 'Self-diffusion in Single-file Pores of Finite Length', J.Chem.Phys., **106** (1997) 8595-8597.

[25] J.M.D. MacElroy and S.-H. Suh., 'Equilibrium and Nonequilibrium Molecular Dynamics Studies of Diffusion in Model One-dimensional Micropores', Micrporous Mesoporous Mat., **48** (2001) 195-202.

[26] K. Hahn and J. Karger, 'Deviations from the normal time regime of single-file diffusion', J.Phys.Chem.B, **102** (1998) 5766-5771.

[27] P.H. Nelson and S.M. Auerbach, 'Self-diffusion in Single-file Membranes is Fickian at Long Times', J. Chem. Phys., **110** (1999) 9235-9243.

[28] J.L. Lebowitz and J.K. Percus, 'Kinetic Equations and Density Expansions: Exactly Solvable One-Dimensional System', Phys. Rev., **155** (1967) 122-138.

[29] I.M. Svishchev and P.G. Kusalik, 'Electrofreezing of Liquid Water: Microscopic Insights', J. Am. Chem. Soc., **118** (1996) 649-654.

[30] N.J. English and J.M.D. MacElroy, 'Hydrogen bonding and molecular mobility in liquid water in external electromagnetic fields', J. Chem. Phys., **119** (2003) 11806-11813.

Table 1. Steady-state permeation rates

Pore (d_p)	j_0 (ns^{-1})	j_E (ns^{-1})	[a] p_0/A_p (nm ns^{-1})	[a] p_E/A_p (nm ns^{-1})
(5,5) (0.689 nm)	1.13 (0.19)	2.60 (0.87)	0.36	0.82
(6,6) (0.820 nm)	2.43 (0.91)	1.53 (0.57)	0.41	0.26
(8,8) (1.104 nm)	6.83 (1.4)	6.33 (0.43)	0.45	0.42
(11,11) (1.502 nm)	25.2 (1.8)	22.4 (1.7)	0.72	0.64

[a] The permeability $p = j/c_w$ with c_w = 33.1 nm^{-3}. The pore cross-sectional area employed here is $(\pi/4)(d_p\text{-}0.34)^2$ where d_p is the carbon centre-carbon centre diameter of the CNT given in the first column. 0.34nm is the Lennard-Jones diameter of the carbon atoms.

Table 2. Intrapore diffusion and partitioning properties

Pore	D_{p0}(nm^2 ns^{-1})	D_{pE}(nm^2 ns^{-1})	$p_0/D_{p0}A_p$ (nm^{-1})	$p_E/D_{pE}A_p$ (nm^{-1})	[b] K_{p0}	[b] K_{pE}
(5,5)	2.09 (0.31)	1.98 (0.12)	0.172	0.414	0.68	1.64
(6,6)	2.35 (0.23)	1.92 (0.17)	0.174	0.135	0.69	0.53
(8,8)	2.68 (0.19)	2.65 (0.48)	0.168	0.158	0.66	0.62
(11,11)	3.74 (0.24)	3.45 (0.54)	0.193	0.186	0.76	0.73

[b] The magnitude of a employed in Equation (11) to compute these values was 0.26nm, the projected length for a given water molecule along the pore axis in the non-field single-file pores..

Figure Captions:

Figure 1. (a,d) Periodic cells simulated for the (5,5) CNT and (11,11) CNT systems respectively: in silver transparent rendering is the CNT with the waters inside represented as van der Waals spheres with the oxygens in red an hydrogens in white. In cyan licorice rendering is the aliphatic chain of the membrane. The polar heads of the phospholipids are represented by van der Waals spheres in blue, red and white. Sticks represent the bulk water. (b,e) Side view of the CNT´s, (5,5) and (11,11) respectively, represented as licorice gray rendering, with the waters molecules, as van der Waals red (oxygens) and white (hydrogens) spheres inside the CNT. (c,f) Top view of the CNT´s, (5,5) and (11,11) respectively represented as licorice gray rendering, with the waters molecules as van der Waals red (oxygens) and white (hydrogens) spheres inside the CNT.

Figure 2. Schematic of the 'black' and 'white' water reservoirs on either side of the CNT, with the CNT oriented along the z-axis, normal to the membrane patch. The concentration of the black water molecules is specified at the edge of the black reservoir (c_1), at the pore mouth (c_2), just inside the pore (c_{2p}), with analogous concentrations on the other side of the simulation cell (the positive z-coordinate half), i.e. c_{3p}, c_3 and c_4. L_c was 3.5 nm in all of the systems simulated.

Figure 3. Axial mean square displacements as a function of time for individual water molecules confined within the pores. The filled squares are sample points for the (5,5) CNT and the open squares are for the (11,11) CNT. The dashed lines represent the linear (Fickian) limit. The results in both cases are for non-field conditions and the results in the presence of the e-field were found to be essentially the same.

Figure 4. Normalised probability distributions of the cosine of the angle which the dipole moment vector of water molecules makes with the positive z-axis, θ. The $\cos\theta$ value is +1 for a water dipole aligned along the +z-axis, and -1 for a water molecule aligned along the –z-axis. The distributions are specified for the bulk water regions, i.e. those in the black and white reservoirs, inside the nanotube and within 4 Å, 4-6 Å and 6-8 Å of the nanotube mouth. (a) (5,5) under zero-field conditions, (b) (5,5) in the field, (c) (6,6) under zero-field conditions, (d) (6,6) in the field, (e) (8,8) under zero-field conditions, (f) (8,8) in the field, (g) (11,11) under zero-field conditions and (h) (11,11) in the field.

Figure 5. Normalized histograms of the number of hydrogen bonds (in black) and water molecules (in gray) inside the CNTs during the MD simulations. (a) (5,5) under zero-field conditions, (b) (5,5) in the field, (c) (6,6) under zero-field conditions, (d) (6,6) in the field, (e) (8,8) under zero-field conditions, (f) (8,8) in the field, (g) (11,11) under zero-field conditions and (h) (11,11) in the field. The time series of these same values indicated a stationary situation without any appreciable drift.

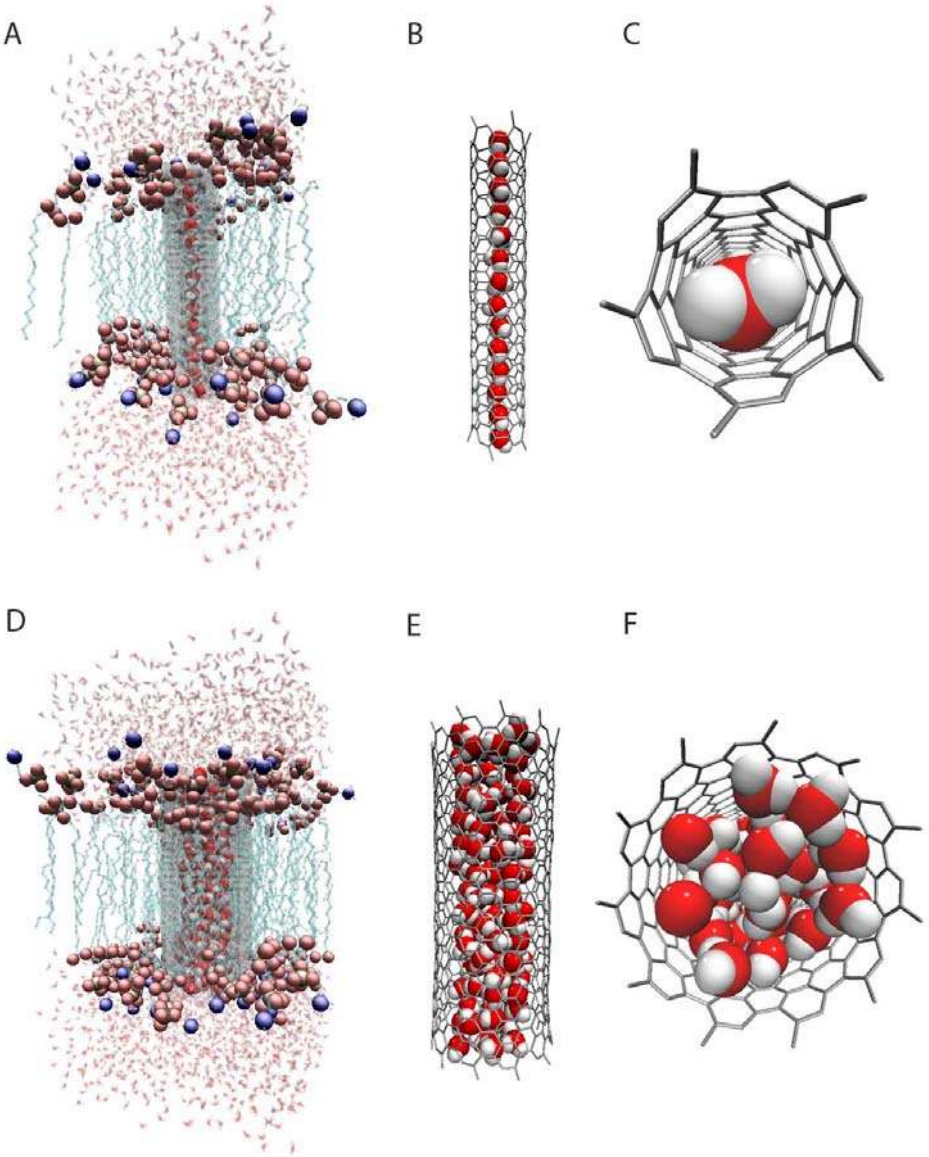

Figure 1.

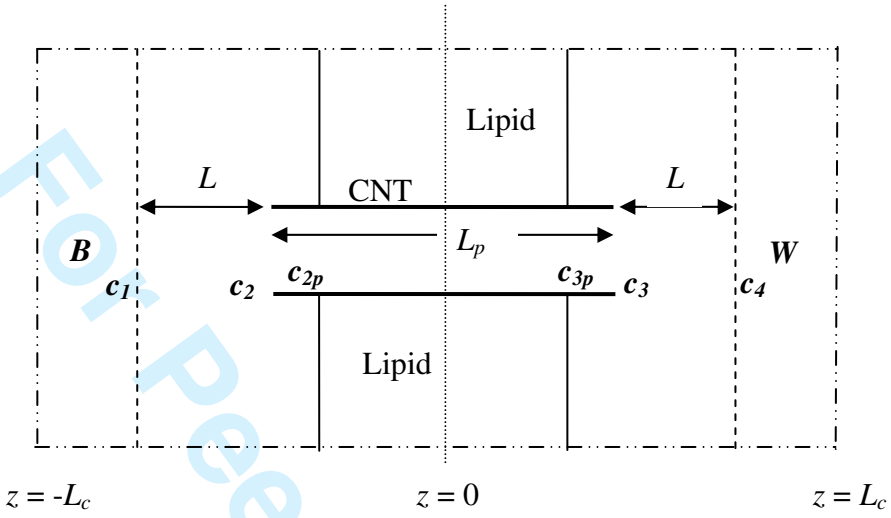

Figure 2.

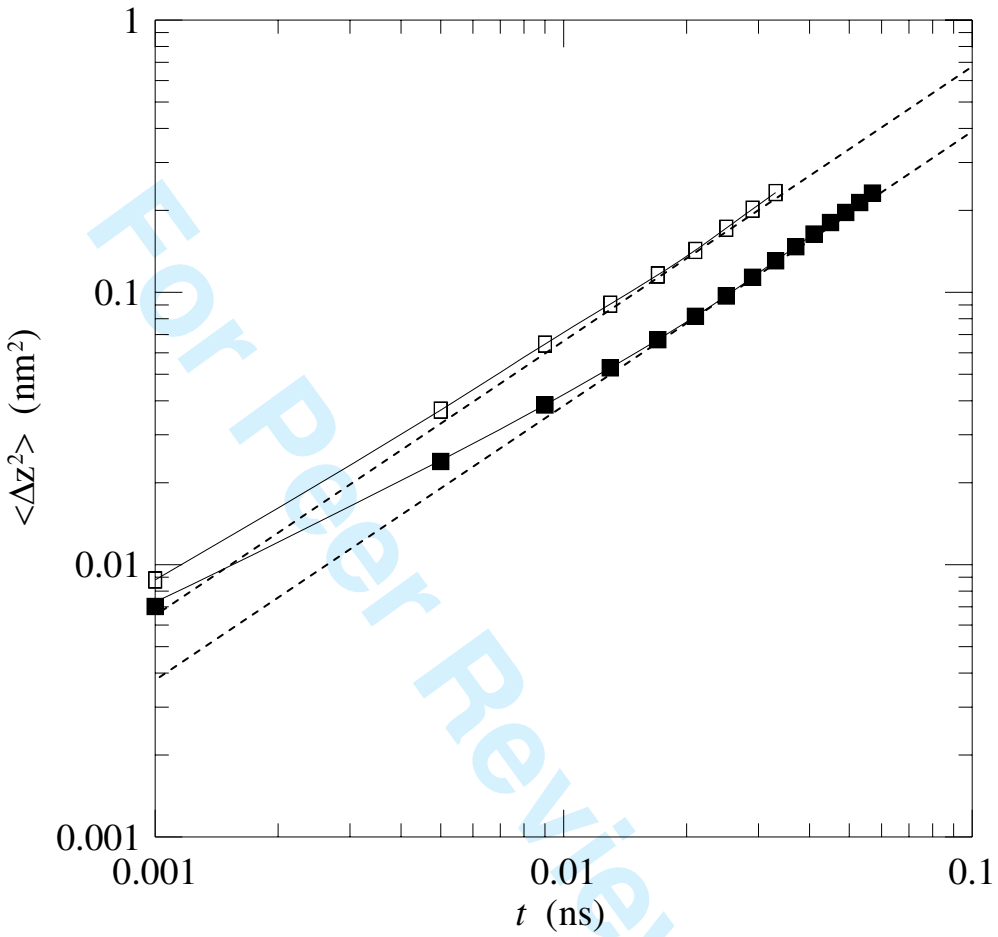

Figure 3

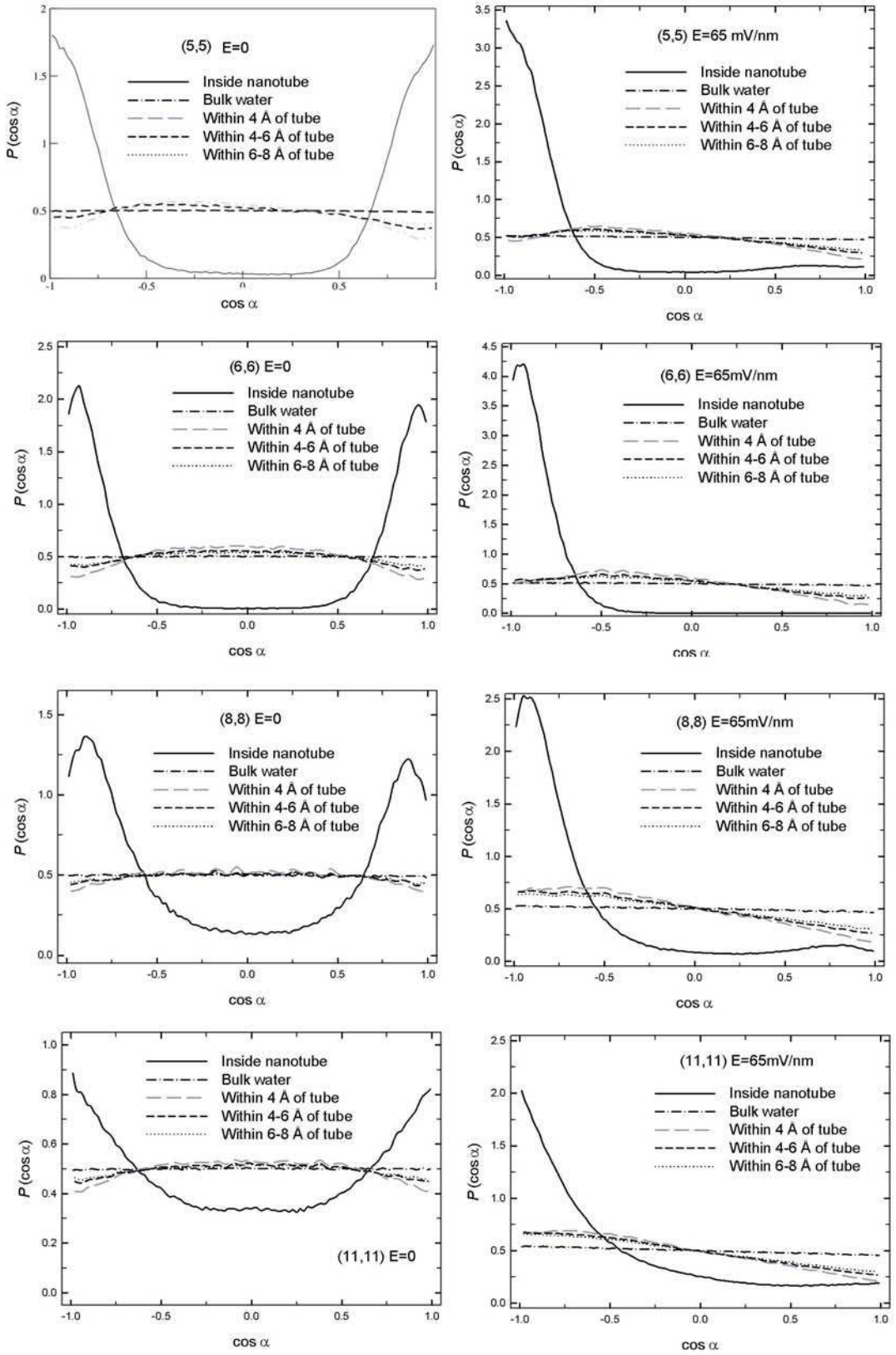
(5,5) E=0
(5,5) E=65 mV/nm
(6,6) E=0
(6,6) E=65mV/nm
(8,8) E=0
(8,8) E=65mV/nm
(11,11) E=0
(11,11) E=65mV/nm
Inside nanotube
Bulk water
Within 4 Å of tube
Within 4-6 Å of tube
Within 6-8 Å of tube
P (cos α)
cos α

Figure 4.

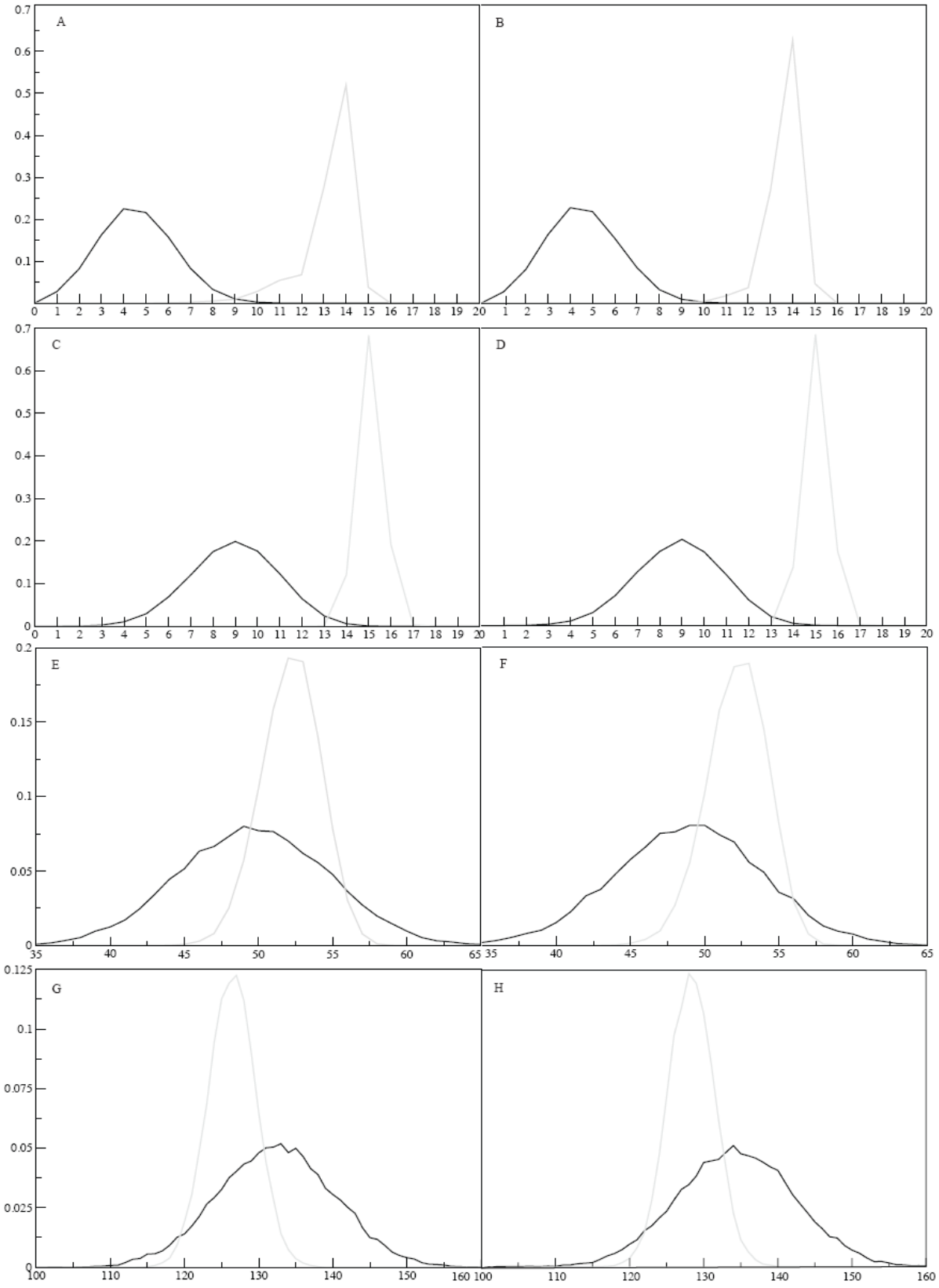

Figure 5.